Supplemental Material to
Synchronization modes in bipartite oscillator networks

Pau Pomés,[1] Bastian Pietras,[1] and Ernest Montbrió[1]

[1]*Department of Engineering, Universitat Pompeu Fabra, 08018 Barcelona, Catalonia, Spain*

CONTENTS

I. General analysis of the bipartite Kuramoto-Sakaguchi model 2
A. Existence of S-states 2
B. Stability of S-states 2
C. Ott-Antonsen equations 3
1. S-state 4
2. PS-states 4

II. From the Quadratic Intregrate-and-Fire model with conductance-based synapses to the E-I Kuramoto-Sakaguchi model 5
A. Reduction using the method of averaging 5
1. The E-I Kuramoto-Sakaguchi model 6
B. Numerical simulations. 7
1. Initial conditions, and evaluation of the Kuramoto order parameter for QIF neurons 7
2. Numerical simulation scheme for QIF neurons 8
C. Phase diagram 9

References 11

I. GENERAL ANALYSIS OF THE BIPARTITE KURAMOTO-SAKAGUCHI MODEL

In this section we perform a general analysis of the bifurcations of the bipartite Kuramoto-Sakaguchi model,

$$\dot{\theta_i}^A = \omega_A - \frac{K_B}{N}\sum_{j=1}^{N}\sin(\theta_i^A - \theta_j^B - \alpha_A), \tag{S1}$$

$$\dot{\theta_i}^B = \omega_B - \frac{K_A}{N}\sum_{j=1}^{N}\sin(\theta_i^B - \theta_j^A - \alpha_B). \tag{S2}$$

We set $\alpha_A = \alpha_B = \alpha$ without loss of generality, and consider $\alpha \in (-\pi/2, \pi/2)$, $\Delta = \omega_A - \omega_B \neq 0$, and $K_A \neq K_B$ with $K_{A,B} > 0$. The results of this section are summarized in the phase diagrams depicted in Fig.S1.

A. Existence of S-states

Setting $\psi_A = \theta_i^A$, $\psi_B = \theta_i^B$, for $i = 1, \ldots, N$, the dynamics of Eqs.(S1,S2) reduce to

$$\dot{\phi} = \Delta - \mathcal{A}\sin(\phi + \phi_0), \tag{S3}$$

for the phase difference $\phi = \psi_A - \psi_B$, where $\Delta = \omega_A - \omega_B$ and

$$\mathcal{A} = \sqrt{K_A^2 + K_B^2 + 2K_AK_B\cos(2\alpha)}, \quad \phi_0 = \arctan\left(\frac{K_A - K_B}{K_A + K_B}\tan\alpha\right).$$

Eq. (S3) is invariant under a permutation of the population indices, $(A, B) \mapsto (B, A)$, or equivalently under

$$(\Delta, \phi, K_A, K_B) \mapsto (-\Delta, -\phi, K_B, K_A). \tag{S4}$$

In addition, Eq. (S3) has a symmetry

$$(\Delta, \phi, \alpha) \mapsto (-\Delta, -\phi, -\alpha). \tag{S5}$$

Hereafter we restrict our analysis to $\alpha \in (0, \pi/2)$ without loss of generality — results for $\alpha \in (-\pi/2, 0)$ can be inferred invoking the symmetry (S5).

For $\mathcal{A} > |\Delta|$, Eq.(S3) has a fixed point (S-state)

$$\phi^* = \arcsin(\Delta/\mathcal{A}) - \phi_0, \tag{S6}$$

and a second fixed point: $\pi - \phi^* - 2\phi_0$. They emerge in a saddle-node (SN) bifurcation at

$$|\Delta|_S = \mathcal{A}, \tag{S7}$$

The S-states exist in the region confined between the thin dotted lines in Fig. S1. The dotted lines correspond to Eq. (S7) for two values of the ratio K_A/K_B.

B. Stability of S-states

For $N = 1$, the linear stability analysis of the fixed point ϕ^* gives one zero eigenvalue, and

$$\mu = d\dot{\phi}/d\phi|_{\phi=\phi^*} = -K_B\cos(\phi^* - \alpha) - K_A\cos(\phi^* + \alpha) = -\sqrt{\mathcal{A}^2 - \Delta^2}. \tag{S8}$$

This eigenvalue determines the linear stability of the S state against perturbations along the ϕ-direction. In addition, for $N > 1$, there are two sets of real $(N-1)$-times degenerated eigenvalues

$$\mu_A = -K_B\cos(\phi^* - \alpha) \tag{S9}$$

and

$$\mu_B = -K_A\cos(\phi^* + \alpha) \tag{S10}$$

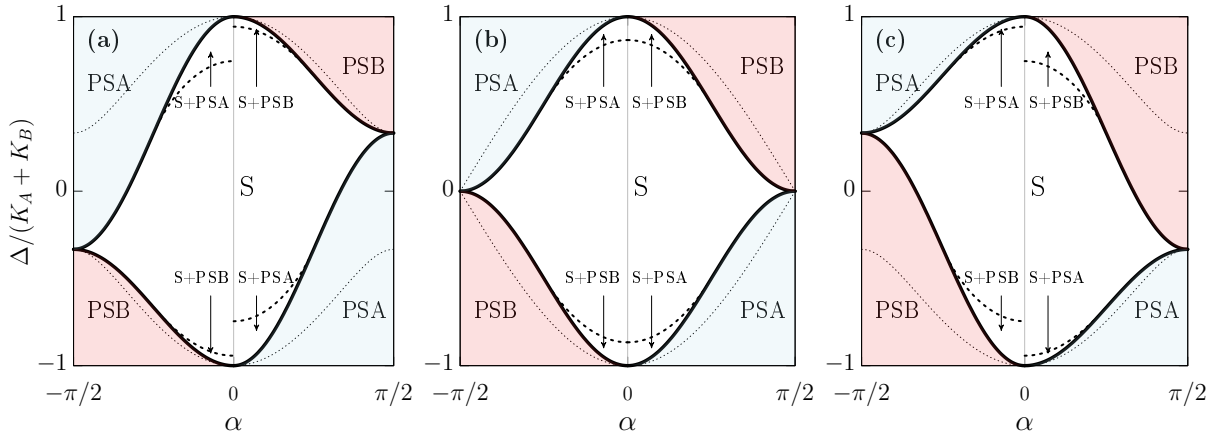


FIG. S1. Phase diagram of the KS model Eqs. (S1,S2) for (a) $K_A = 2K_B$, (b) $K_A = K_B$ and (c) $K_A = K_B/2$. Shaded regions: PS-states are the only stable attractor. Red-shaded regions (PSB): The instability of the S-state is through the disintegration of B-oscillators. Blue-shaded regions (PSB): The instability of the S-state is through the disintegration of A-oscillators. White region (S): The S-state is stable. Solid black lines: Stability boundaries of the S-state, Eqs.(S15,S13). Dashed lines: SN bifurcations where PS-states are born ($N \to \infty$), Eqs.(S21,S23). Thin-dotted lines, Eq. (S7): SN boundaries where the S-state is born.

These eigenvalues describe the internal stability of the in-phase synchronized oscillators in populations A and B, respectively. The eigenvalues satisfy the relation

$$\mu = \mu_A + \mu_B, \tag{S11}$$

which implies that the S-state may only become unstable via the disintegrateion of oscillators in population A or B, except when $\alpha = 0$. We denote the two possible emerging PS states as PSA or PSB.

Evaporation of population A: Setting $\mu_A = 0$ and $\mu_B < 0$, we find the critical phase at which the population A disintegrates,

$$\phi^* = \alpha - \pi/2, \tag{S12}$$

while the population B remains in-phase synchronized, $\mu_B = -K_B \sin(2\alpha)$. Substituting Eqs. (S8,S12) into Eq. (S11) yields the loci of the instability

$$\Delta_A = -K_B - K_A \cos(2\alpha). \tag{S13}$$

Evaporation of population B: By applying the permutation symmetry Eq. (S4) to Eqs. (S12,S13), we find

$$\phi^* = -\alpha + \pi/2, \tag{S14}$$

and

$$\Delta_B = K_A + K_B \cos(2\alpha) \tag{S15}$$

The phase diagrams shown in Fig. S1 show the instability boundaries $\Delta_{A,B}$ and the SN boundary Δ_S for different values of the ratio K_A/K_B. These boundaries are valid for $\alpha \in [0, \pi/2)$. Using the symmetry Eq. (S5), we recover the instability boundaries for $\alpha \in [-\pi/2, 0)$. These four bifurcation boundaries are depicted in Fig. S1 using solid lines.

C. Ott-Antonsen equations

The reduced Ott-Antonsen equations corresponding to Eqs.(S1,S2) are a trivial generalization of Eqs. (10-12) in the main text:

$$\dot{r}_A = \frac{K_B r_B}{2}(1 - r_A^2)\cos(\phi - \alpha), \tag{S16}$$

$$\dot{r}_B = \frac{K_A r_A}{2}(1 - r_B^2)\cos(\phi + \alpha), \tag{S17}$$

$$\dot{\phi} = \Delta - K_A r_A \frac{1 + r_B^2}{2r_B}\sin(\phi + \alpha) - K_B r_B \frac{1 + r_A^2}{2r_A}\sin(\phi - \alpha). \tag{S18}$$

Note that Eqs. (S16-S18) are invariant under Eq. (S5):

$$(\Delta, \phi, \alpha) \mapsto (-\Delta, -\phi, -\alpha).$$

In addition, the OA equations also have the permutational symmetry

$$(\Delta, \phi, K_A, K_B, r_A, r_B) \mapsto (-\Delta, -\phi, K_B, K_A, r_B, r_A). \tag{S19}$$

1. S-state

Setting $r_1 = r_2 = 1$ in Eqs. (S16-S18), we find that $\dot{r}_A = \dot{r}_B = 0$, and Eq. (S18) becomes Eq.(S3). The Jacobian matrix corresponding to Eqs. (S16-S18) evaluated at the fixed point $(r_A, r_B, \phi) = (1, 1, \phi^*)$ is triangular, with three (real) eigenvalues: μ, μ_A, and μ_B. Hence, the stability of the S-state of Eqs. (S16-S18) coincides with that of the finite-size system analyzed above.

2. PS-states

Considering $r_A = 1$ and $r_B \in (0, 1)$, Eq. (S17) gives the critical phase Eq. (S14). Setting $\dot{\phi} = 0$ yields

$$r_B = \frac{K_A}{\Delta \pm \sqrt{\Delta^2 - K_A^2 - 2K_A K_B \cos(2\alpha)}}. \tag{S20}$$

The PSB and the S-state meet at $(r_A, r_B, \phi^*) = (1, 1, \pi/2 - \alpha)$, when Eq. (S15) is fulfilled. The instability of the S-state is hence through a transcritical bifurcation (TC) with the PSB state. In addition, the fixed points Eq. (S20) originate in a SN bifurcation, with $r_B = K_A/\Delta$. This bifurcation is only observed in the original system of Eqs. (S1,S2) if $r_B \in (0, 1]$, i.e. $\Delta \geq K_A$. The SN bifurcating boundary is

$$\Delta_{PSB} = \sqrt{K_A^2 + 2K_A K_B \cos(2\alpha)}, \quad \text{for } \alpha \in (0, \pi/4). \tag{S21}$$

The SN bifurcation line tangentially meets the TC bifurcating line Eq. (S15) at the Saddle-Node-Transcritical (SNTC) codimension-two point $(\Delta\omega, \alpha) = (K_A, \pi/4)$.

The complementary case, $r_B = 1$ and $r_A \in (0, 1)$, is recovered by invoking the symmetry Eq. (S19) to Eqs. (S20),

$$r_A = \frac{K_B}{-\Delta \pm \sqrt{\Delta^2 - K_B^2 - 2K_A K_B \cos(2\alpha)}}, \tag{S22}$$

and to Eqs. (S21)

$$\Delta_{PSA} = -\sqrt{K_B^2 + 2K_A K_B \cos(2\alpha)}, \quad \text{for } \alpha \in (0, \pi/4). \tag{S23}$$

The SN boundaries Eqs. (S21,S23) are valid for $\alpha \in [0, \pi/2)$. Using the symmetry Eq. (S5), we recover the SN bifurcating lines for $\alpha \in [-\pi/2, 0)$. All these bifurcation boundaries are depicted in Fig. S1 using dashed lines.

II. FROM THE QUADRATIC INTREGRATE-AND-FIRE MODEL WITH CONDUCTANCE-BASED SYNAPSES TO THE E-I KURAMOTO-SAKAGUCHI MODEL

In this section, use the method of averaging to reduce a population of QIF neurons to the Kuramoto-Sakaguchi model. The approach is similar to that of Ref. [1], but instead of analyzing a QIF network with *current-based* synapses, here instead we consider a population with *conductance-based synapses*.

The equations governing the evolution of the membrane potential V of a population of QIF neurons globally coupled via conductance-based synapses read [2, 3]

$$\tau \dot{V}_i = V_i^2 + \eta + \tau \frac{g\epsilon}{N} \sum_{j=1}^{N} \sum_k \delta(t - t_j^{(k)}) \left[E - V_i\right]; \quad j = 1, \ldots, N. \tag{S24}$$

The neuron's membrane time constant is τ, and parameter $\eta > 0$ controls the natural frequency of the neurons. The resetting rule is as follows: Each time V_j reaches ∞ in Eq. (S24), the neuron emits a spike and V_j^σ is reset to $-\infty$. Neurons are globally coupled with synaptic strength $g > 0$, and E is the synaptic reversal potential. The event $t_j^{(k)}$ is the time of the kth spike of the jth neuron, and $\delta(t)$ is the Dirac delta function. Finally, $\epsilon > 0$ is a parameter introduced for mathematical convenience.

A. Reduction using the method of averaging

We first consider an isolated, regularly spiking QIF neuron (i.e. $g = 0$). Then, the solution of the QIF model

$$\tau \dot{V} = V^2 + \eta \tag{S25}$$

immediately after a spike, $V(0) = -\infty$, is

$$V(t) = \sqrt{\eta} \tan\left(t\sqrt{\eta}/\tau - \pi/2\right). \tag{S26}$$

The frequency of the neuron is

$$\Omega = 2\sqrt{\eta}/\tau, \tag{S27}$$

and a phase variable θ can be defined in the interval $[0, 2\pi)$ as

$$\theta = \Omega t = 2\arctan(V/\sqrt{\eta}) + \pi. \tag{S28}$$

Next, we assume that the neuron is perturbed so that its membrane potential instantaneously changes from V to $V + \delta V$. Then, the new phase after the perturbation is $\theta_{new} = 2\arctan((V + \delta V)/\sqrt{\eta}) + \pi$, and the neuron's PRC is

$$\text{PRC}(\theta, \delta V) = \theta_{new} - \theta = 2\arctan(\delta V/\sqrt{\eta} - \cot(\theta/2)) + \pi - \theta. \tag{S29}$$

This function depends on both the strength of the perturbation and the phase of the neuron at the instant of the perturbation.

Weak perturbations produce small changes in the membrane potential, $|\delta V| \ll 1$. Then the PRC scales linearly with the strength of the perturbation [2, 4]

$$\text{PRC}(\theta, \delta V) \approx Z(\theta)\delta V,$$

where $Z(\theta)$ is called phase sensitivity, or infinitesimal phase resetting curve

$$Z(\theta) = \left.\frac{\partial \text{PRC}(\theta, \delta V)}{\partial(\delta V)}\right|_{\delta V = 0} = \frac{1 - \cos\theta}{\sqrt{\eta}}. \tag{S30}$$

When weak perturbations are described by a continuous function $P(t)$ with $|P(t)| \ll 1$, the infinitesimal change in the phase due to the perturbations is $d\theta = Z(\theta)P(t)dt$. Then, if $\epsilon \ll 1$, Eq. (S24) is well approximated by the so-called Winfree model

$$\dot{\theta}_i = \Omega + \frac{g\epsilon}{N} \sum_{j=1}^{N} \frac{2\delta(\theta_j)}{\tau} \left[E(1 - \cos\theta_i) + \sqrt{\eta}\sin\theta_i\right], \tag{S31}$$

where we have written the perturbations to the neuron due to the synaptic inputs from the other neurons in terms of the phase variables Eq. (S28), and used the trigonometric identities $\tan(x/2-\pi/2) = -\cot(x/2) = -\sin x/(1-\cos x)$. Recall that $\theta_j \in [0, 2\pi)$, so that the Dirac delta function in Eq. (S31) has argument zero whenever the inhibitory neuron fires.

The assumption of weak coupling allows for a separation of time scales so that the phases can be written as

$$\theta_i = \Phi + \varphi_i, \tag{S32}$$

where Φ describes the fast, free-running oscillation of period $T = 2\pi/\Omega$, and the phases φ_i describe slow phase drifts produced by synaptic inputs. Then, substituting Eq. (S32) into Eq. (S31) we find the evolution equation for the slow phases

$$\dot{\varphi}_i = 2\frac{g\epsilon}{\tau N}\sum_{j=1}^{N}\delta(\Phi+\varphi_j)\left[E(1-\cos(\Phi+\varphi_i)) + \sqrt{\eta}\sin(\Phi+\varphi_i)\right] \tag{S33}$$

Next we average the r.h.s. of Eq. (S33) over one period of the fast oscillation, T, considering that the slow phases φ_i remain constant. Then, Eq. (S33) reduces to

$$\dot{\varphi}_i = \frac{g\epsilon}{N\tau\pi}\sum_{j=1}^{N}\left[E(1-\cos(\varphi_i-\varphi_j)) + \sqrt{\eta}\sin(\varphi_i-\varphi_j)\right]. \tag{S34}$$

In terms of the original phases Eq. (S32), and using the definitions

$$K = \frac{g\epsilon}{\tau\pi}\sqrt{\eta+E^2}; \quad \tan\alpha = \frac{E}{\sqrt{\eta}}; \quad \omega = \frac{2\sqrt{\eta}}{\tau} + \frac{\epsilon g E}{\pi\tau}, \tag{S35}$$

we obtain the Kuramoto-Sakaguchi (KS) model corresponding to a population of QIF neurons with recurrent conductance-based synapses:

$$\dot{\theta}_i = \omega + \frac{K}{N}\sum_{j=1}^{N}\sin(\theta_i-\theta_j-\alpha). \tag{S36}$$

Note that the fully synchronized state $\theta_i = \psi$, for $i = 1, \ldots, N$ is not stable in this model.

1. The E-I Kuramoto-Sakaguchi model

The evolution equations of a bipartite E-I network of identical QIF neurons are

$$\tau\dot{V_i^I} = \left(V_i^I\right)^2 + \eta + \tau\frac{g\epsilon}{N}\sum_{j=1}^{N}\sum_{k}\delta(t-t_j^{(k),E})\left[E_E - V_i^I\right], \tag{S37}$$

$$\tau\dot{V_i^E} = \left(V_i^E\right)^2 + \eta + \tau\frac{g\epsilon}{N}\sum_{j=1}^{N}\sum_{k}\delta(t-t_j^{(k),I})\left[E_I - V_i^E\right], \tag{S38}$$

where the reversal potentials of excitatory and inhibitory synapses are $E_E > 0$ and $E_I < 0$, respectively. Note that all neurons have the same intrinsic parameter $\eta > 0$ and thus have the same natural frequency. Using the results of the previous section, we write the corresponding Sakaguchi-Kuramoto bipartite model

$$\dot{\theta_i^I} = \frac{2\sqrt{\eta}}{\tau} + \frac{g\epsilon}{\tau\pi}\left[E_E + \frac{\sqrt{\eta+E_E^2}}{N}\sum_{j=1}^{N}\sin\left(\theta_i^I - \theta_j^E - \alpha_E\right)\right],$$

$$\dot{\theta_i^E} = \frac{2\sqrt{\eta}}{\tau} + \frac{g\epsilon}{\tau\pi}\left[E_I + \frac{\sqrt{\eta+E_I^2}}{N}\sum_{j=1}^{N}\sin\left(\theta_i^E - \theta_j^I - \alpha_I\right)\right].$$

where

$$\alpha_{E,I} = \arctan(E_{E,I}/\sqrt{\eta}) \tag{S39}$$

Redefining the phases as

$$\theta_i^I = \theta_i^A; \quad \theta_i^E = \theta_i^B + \pi + \frac{\alpha_I - \alpha_E}{2}, \tag{S40}$$

we obtain

$$\dot{\theta_i^A} = \frac{2\sqrt{\eta}}{\tau} + \frac{g\epsilon}{\pi\tau} E_E - \frac{g\epsilon\sqrt{\eta + E_E^2}}{\pi\tau} \frac{1}{N} \sum_{j=1}^{N} \sin\left(\theta_i^A - \theta_j^B - \alpha\right), \tag{S41}$$

$$\dot{\theta_i^B} = \frac{2\sqrt{\eta}}{\tau} + \frac{g\epsilon}{\pi\tau} E_I - \frac{g\epsilon\sqrt{\eta + E_I^2}}{\pi\tau} \frac{1}{N} \sum_{j=1}^{N} \sin\left(\theta_i^B - \theta_j^A - \alpha\right), \tag{S42}$$

where we defined

$$\alpha = \frac{\alpha_E + \alpha_I}{2}. \tag{S43}$$

The KS model Eqs. (S41,S42) has the form of Eqs. (1) in the main text, Eqs. (S1,S2), with

$$K_A = \frac{g\epsilon\sqrt{\eta + E_I^2}}{\tau\pi}; \quad K_B = \frac{g\epsilon\sqrt{\eta + E_E^2}}{\tau\pi}. \tag{S44}$$

and

$$\omega_A = \frac{2\sqrt{\eta}}{\tau} + \frac{g\epsilon}{\pi\tau} E_E; \quad \omega_B = \frac{2\sqrt{\eta}}{\tau} + \frac{g\epsilon}{\pi\tau} E_I,$$

and

$$\Delta = \omega_A - \omega_B = \frac{g\epsilon}{\pi\tau}(E_E - E_I). \tag{S45}$$

Note that despite the fact that QIF neurons are assumed to be identical, the different nature of the neurons (reflected in different excitatory and inhibitory synaptic reversal potentials) results in parameter asymmetries ($\omega_A \neq \omega_B$, $K_A \neq K_B$, $\alpha_E \neq \alpha_I$) in the reduced KS model.

B. Numerical simulations.

Figure. S2 shows two numerical simulations of an E-I bipartite network QIF neurons Eqs. (S37,S38) with $N = 100$ for two values of the effective coupling strength $g\epsilon$. In addition, we also show numerical simulations of low-dimensional, Ott-Antonsen (OA) Eqs. (S16-S18), which can be compared with the E-I QIF model via Eqs.(S39,S40,S43-S45).

Panels Fig. S2(a1,b1) show the time-evolution of the Kuramoto order parameters of both E and I populations using red and blue lines, respectively. Solid and dashed lines correspond QIF and the KS models, respectively. Note that the agreement between the models increases as $g\epsilon \to 0$, as expected from the averaging approximation.

Figs. S2(a1,b1) show that initially the populations are not fully synchronous. After a transitory period, the cross-talk between E and I neurons leads to full synchrony in the I population ($r_I = 1$) while the E population displays partial synchrony ($r_E < 1$) — we refer to this state as PS_E. In panels Fig. S2(a2,b2) we show raster plots corresponding to the last 20 time units of the simulation of E-I QIF network (only the spike events of $N = 8$ neurons in each population are shown). Note that excitatory neurons fire sparsely, with a low firing rate compared to I-neurons, in consonance with experimental evidence [3, 5]. Note that this effect enhances with $g\epsilon$, as the inhibitory input to E-neurons increases. Furthermore, I-neurons increase their firing rate (and hence their input to E-neurons) due to the increased excitatory drive with $g\epsilon$.

1. *Initial conditions, and evaluation of the Kuramoto order parameter for QIF neurons*

To evaluate the Kuramoto order parameters in the E-I network of QIF neurons, we used Eq. (S28) to transform voltages into phases, and then we evaluated the Kuramoto order parameters as $z_{E,I} = r_{E,I} e^{i\psi_{E,I}} = N^{-1} \sum_{j=1}^{N} e^{i\theta_j^{E,I}}$. In addition, we initialized the neurons' phases in the the Ott-Antonsen manifold [6] as

$$\theta_i^{E,I} = 2 \arctan\left(\frac{1 - r_{E,I}}{1 + r_{E,I}} \tan\left[\pi\left(\frac{i}{N} - \frac{1}{2}\right)\right]\right) + \psi_{E,I}, \quad i \in [1, N]. \tag{S46}$$

for a given initial value of the Kuramoto order parameters $z_{E,I}$.

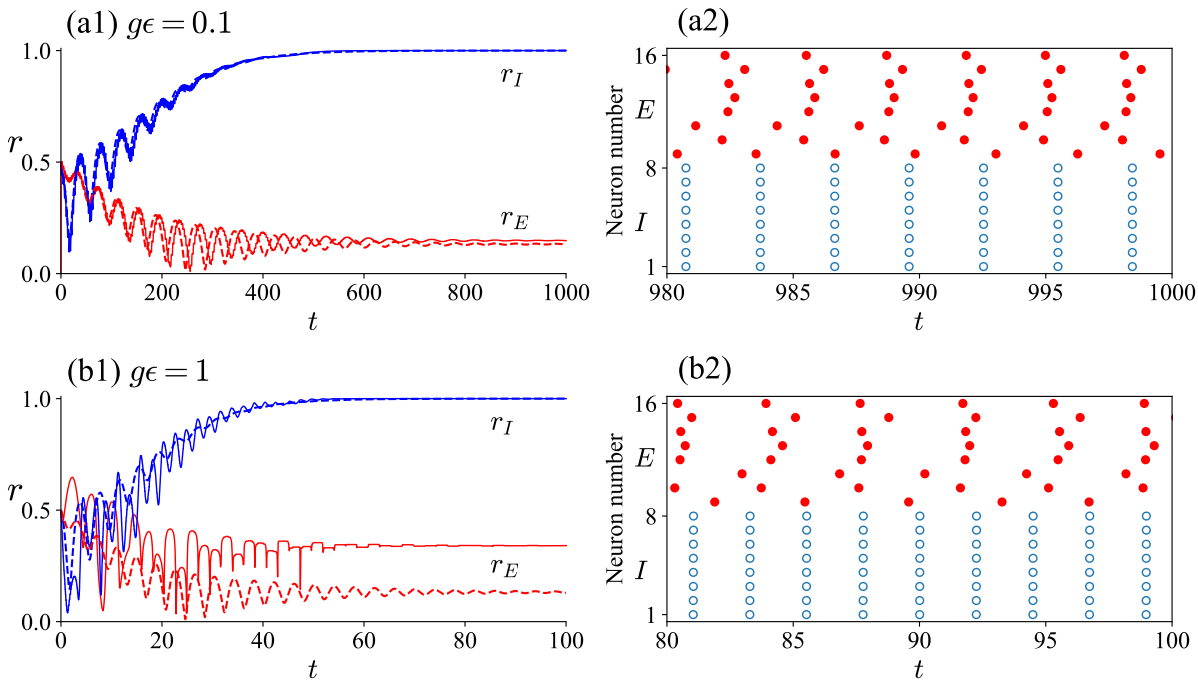


FIG. S2. Numerical simulations of a bipartite $E - I$ network of QIF neurons Eqs. S37,S38), and of the Ott-Antonsen (OA) Eqs. (S16-S18). Panels (a1,b1) Evolution of the Kuramoto Order Parameters of the E and I populations, for $g\epsilon = 0.1$ (a1), $g\epsilon = 1$ (b1). Solid lines: E-I QIF model. Dashed lines: OA model. Panels (a2,b2): Raster plots of the E-I QIF network for $g = 0.1$ (a2) and $g\epsilon = 1$ (b2). Only the spike times of $N = 8$ randomly selected neurons are shown. Parameters: $E_E = 5$, $E_I = -1$, $\eta = 1$, $\tau = 1$. Initial conditions: $r_I = r_E = 0.5$ and $\psi_I = \psi_E = 0$. Parameters OA model: using Eqs.(S43-S45). Initial conditions OA model (using Eq.(S40)): $r_A = r_B = 0.5$, $\psi_A = 0$ and $\psi_B = -\pi - (\arctan E_I - \arctan E_E)/2$.

2. *Numerical simulation scheme for QIF neurons*

To obtain the results in Fig. S2, we used an event-driven numerical scheme, using Eq. (S46). The procedure is as follows:

1. Identify the neuron with the largest phase θ_i^σ ($\theta_i^\sigma \in [0, 2\pi)$)

2. Compute the time remaining until this neuron fires:

$$\Delta t = \frac{2\pi - \theta_i^\sigma}{\Omega},$$

, where Ω is given by Eq. (S27).

3. Advance the simulation time to the spike event,

$$t \to t + \Delta t,$$

and update all neuron phases according to

$$\theta_j^{E,I} \to \theta_j^{E,I} + \Omega \cdot \Delta t.$$

Then, reset the neuron:

$$\theta_i^\sigma \to 0.$$

4. Update the phases of all neurons in population σ' in response to the spike emitted by neuron θ_i^σ:

$$\theta_j^{\sigma'} \to \theta_j^{\sigma'} + \mathrm{PRC}\left(\theta_j^{\sigma'}, \delta V_j^{\sigma'}\right),$$

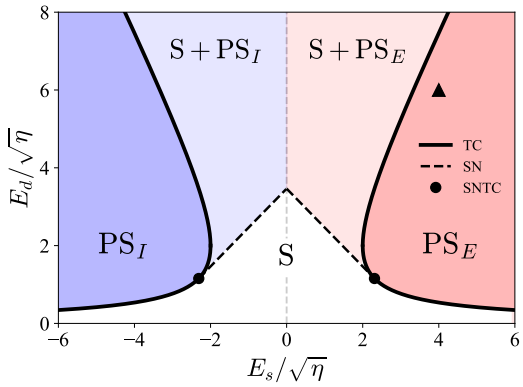


FIG. S3. Phase diagram of the E-I Kuramoto-Sakaguchi model Eqs.(S41,S42). Solid lines: Stability boundaries of the S state, Eqs. (S50,S52). In the OA reduced equations this corresponds to a transcritical (TC) bifurcation. Dashed black lines: Saddle Node (SN) bifurcations where PS-states are born, Eqs. (S51,S53). Shaded-regions: PS-states exist, either in isolation of coexisting with the S-state (light-shaded). Blue and Red shading signals desynchronization of the Inhibitory (PS$_I$) and the Excitatory (PS$_E$) populations, respectively. TC and SN bifurcating lines meet in the SNTC codimension-two points $(E_s/\sqrt{\eta}, E_d/\sqrt{\eta})\big|_{SNTC} = (\pm 4/\sqrt{3}, 2/\sqrt{3})$. Symbol "▲": Parameters used in Fig. S2: $E_E = 5$, $E_I = -1$, $\eta = 1$.

where $\mathrm{PRC}(\theta_j^{\sigma'}, \delta V_j^{\sigma'})$ is defined in Eq. (S29), and [1]

$$\delta V_j^{\sigma'} = \left(1 - e^{-g\epsilon/N}\right)\left[E_\sigma - \sqrt{\eta}\tan\left(\frac{\theta_j^{\sigma'} - \pi}{2}\right)\right]. \tag{S47}$$

5. Repeat steps 1–4 until the end of the simulation time t.

C. Phase diagram

In this section, we use the results of the bifurcation analysis of the bipartite KS model Eqs. (S1,S2) —- shown in Section 1 — to represent the phase diagram of the E-I KS model, Eqs. (S41,S42), see Fig. S3. This diagram allows for a direct interpretation of the dynamics of the KS model in terms of the parameters of an E-I QIF network. Note that the phase diagram is independent of the coupling strength $g\epsilon$, and that it is expected to represent the actual dynamics of the E-I QIF network only in the limit $g\epsilon \to 0$.

To represent the stability boundaries in terms of the original parameters of the QIF model, we define two new parameters

$$E_s = E_E + E_I; \quad E_d = E_E - E_I. \tag{S48}$$

Note that $E_s = 0$ (vertical dashed line in Fig. S3) represents a network with fully balanced excitation and inhibition. In terms of the parameters of the KS model, this corresponds to $K_A = K_B$, and $\alpha = 0$. Then, Eqs.(S8,S9,S10) reduce to

$$\mu_A = \mu_B = \mu < 0, \tag{S49}$$

and instabilities of the S-state are not possible.

S-states: In terms of the parameters of the QIF model, the SN boundary Eq.(S7) where S-states are born corresponds to

$$\eta = 0.$$

The eigenvalue Eq. (S8) shows that stable S-States exist for all $\eta > 0$, provided that $\epsilon g \neq 0$. Recall that neurons in the e i model Eqs. (S37,S38) have identical intrinsic parameters η.

---

[1] Since spikes are instantaneous, the intrinsic QIF dynamics of the postsynaptic neuron can be neglected ($V^2 + \eta \to 0$) and Eq. (S24) can then be integrated analytically (for a single spike) by separation of variables, obtaining $V_{new} = E - (E - V)e^{-g\epsilon/N}$. Then $\delta V = V_{new} - V$ and we use Eq. (S28) to express the result in terms of the neuron phases, resulting in Eq (S47).

Disintegration of the Inhibitory population (A-population): The instability boundary Eq. (S13) in terms of the parameters of the QIF model can be expressed as

$$\eta_A = -\frac{1}{4}E_d^2 - \frac{1}{2}E_s E_d, \tag{S50}$$

and the SN bifurcation boundary, Eq. (S23), is

$$\eta_{PSA} = \frac{1}{12}\left(E_d - E_s\right)^2. \tag{S51}$$

Disintegration of the Excitatory population (B-population): The instability boundary Eq.(S15) in terms of the parameters of the QIF model is

$$\eta_B = -\frac{1}{4}E_d^2 + \frac{1}{2}E_s E_d, \tag{S52}$$

The SN bifurcation boundaries (S21), are

$$\eta_{PSB} = \frac{1}{12}\left(E_d + E_s\right)^2 \tag{S53}$$

The SN and TC boundaries Eqs. (S50,S51) and Eqs. (S52,S53), meet in the Saddle-Node-Transcritical codimension-two point

$$\eta_{SNTC} = \frac{3}{4}E_d^2 = \frac{3}{16}E_s^2. \tag{S54}$$

Figure S3 shows the phase diagram with the boundaries Eqs. (S50-S53). For $E_s > 0$, excitation dominates over inhibition, which promotes the desynchronization of the excitatory population (PS_E-state). Using Eq.(S40) to write the phase difference between the populations in the PSB state, Eq. (S14), in terms of the original phases, we find:

$$\psi_I - \psi_E = -\pi/2 - \alpha_I,$$

and hence excitation precedes inhibition with a phase difference in $[-\pi/2, 0)$.

By contrast, for networks with dominating inhibition, $E_s < 0$, PS-states are characterized by desynchronization of inhibitory neurons. Using Eq.(S40) to write the phase difference between the populations in the PSA state Eq. (S12), in terms of the original phases, $\psi_A - \psi_B = \psi_I - \psi_E + \pi + (\alpha_I - \alpha_E)/2$, we find:

$$\psi_I - \psi_E = \pi/2 + \alpha_E,$$

and hence, inhibition precedes excitation with a phase difference in $[\pi/2, \pi)$.

[1] Pau Clusella, Bastian Pietras, and Ernest Montbrió, "Kuramoto model for populations of quadratic integrate-and-fire neurons with chemical and electrical coupling," Chaos: An Interdisciplinary Journal of Nonlinear Science **32**, 013105 (2022).
[2] E. M. Izhikevich, *Dynamical Systems in Neuroscience* (The MIT Press, Cambridge, Massachusetts, 2007).
[3] Christoph Börgers, *An introduction to modeling neuronal dynamics*, Vol. 66 (Springer, 2017).
[4] A. T. Winfree, "Biological rhythms and the behavior of populations of coupled oscillators." J. Theor. Biol. **16**, 15–42 (1967).
[5] M.A. Whittington, R.D. Traub, N. Kopell, B. Ermentrout, and E.H. Buhl, "Inhibition-based rhythms: experimental and mathematical observations on network dynamics," Int. Journal of Psychophysiol. **38**, 315 – 336 (2000).
[6] E. Ott and T. M. Antonsen, "Low dimensional behavior of large systems of globally coupled oscillators," Chaos **18**, 037113 (2008).